

Article

Open Access



The integration of $\text{LiNi}_{0.8}\text{Co}_{0.1}\text{Mn}_{0.1}\text{O}_2$ coatings on separators for elevated battery performance

Modeste Venin Mendieev Nitou^{1,2}, Xiaodong Fang¹, Jiaqi Wang^{1,3}, Rui Liu^{1,3}, Yashuai Pang¹, Yinghua Niu^{1,2,3,*}, Wu Qin⁴, Chao Zhao^{5,*}, Yuanfu Chen^{2,*}, Zhen Zhang⁵, Weiqiang Lv^{1,3,*}

¹School of Physics, University of Electronic Science and Technology of China, Chengdu 611731, Sichuan, China.

²School of Integrated Circuit Science and Engineering (Exemplary School of Microelectronics), Chengdu 611731, Sichuan, China.

³Yangtze Delta Region Institute (Huzhou), University of Electronic Science and Technology of China, Huzhou 313001, Zhejiang, China.

⁴National Engineering Laboratory for Biomass Power Generation Equipment, School of Renewable Energy Engineering, North China Electric Power University, Beijing 102206, China.

⁵School of Chemical Engineering and Technology, Center for Biosafety Research and Strategy, Tianjin University, Tianjin 300072, China.

***Correspondence to:** Dr. Yinghua Niu, School of Physics, University of Electronic Science and Technology of China, No. 2006, Xiyuan Ave, West Hi-Tech Zone, Chengdu 611731, Sichuan, China. E-mail: yh_niu@uestc.edu.cn; Dr. Yuanfu Chen, School of Integrated Circuit Science and Engineering (Exemplary School of Microelectronics), Chengdu 611731, Sichuan, China. E-mail: yfchen@uestc.edu.cn; Dr. Weiqiang Lv, School of Physics, University of Electronic Science and Technology of China, No. 2006, Xiyuan Ave, West Hi-Tech Zone, Chengdu 611731, Sichuan, China. E-mail: eselwq@uestc.edu.cn; Dr. Chao Zhao, School of Chemical Engineering and Technology, Center for Biosafety Research and Strategy, Tianjin University, No. 92, Weijin Road, Tianjin 300072, China. E-mail: zhao_chao@tju.edu.cn

How to cite this article: Nitou, M. V. M.; Fang, X.; Wang, J.; Liu, R.; Pang, Y.; Niu, Y.; Qin, W.; Zhao, C.; Chen, Y.; Zhang, Z.; Lv, W. The integration of $\text{LiNi}_{0.8}\text{Co}_{0.1}\text{Mn}_{0.1}\text{O}_2$ coatings on separators for elevated battery performance. *Energy Mater.* 2025, 5, 500018. <https://dx.doi.org/10.20517/energymater.2024.105>

Received: 3 Aug 2024 **First Decision:** 12 Oct 2024 **Revised:** 27 Oct 2024 **Accepted:** 31 Oct 2024 **Published:** 10 Jan 2025

Academic Editor: Jiazhao Wang **Copy Editor:** Fangling Lan **Production Editor:** Fangling Lan

Abstract

Improving the efficiency and safety of lithium-ion batteries (LIBs) with high-energy cathodes is crucial, yet challenging due to the limitations of commercial separators. Herein, we find that “giving” a portion of the Ni-rich $\text{LiNi}_{0.8}\text{Co}_{0.1}\text{Mn}_{0.1}\text{O}_2$ (NCM811) positive electrode to the Al_2O_3 -coated polyethylene (PE) ($\text{PE}/\text{Al}_2\text{O}_3$) separator as an active and thick ceramic coating ($> 10 \mu\text{m}$) can more efficiently enhance the separator’s wettability and thermal stability compared with the inert and thin ($< 5 \mu\text{m}$, typically 1–2 μm) Al_2O_3 coating. The NCM811 coating on the separator can take part in the electrochemical reaction and contribute capacity without increasing the cell dead weight. The NCM811-coated separator has a low thermal shrinkage of 0.8% at 160 °C and a high lithium-ion transfer number of 0.66. Notably, the NCM811-coated separator enhances electrochemical performance, delivering higher capacities compared to traditional PE and $\text{PE}/\text{Al}_2\text{O}_3$ separators. Furthermore, it effectively mitigates lithium



© The Author(s) 2025. **Open Access** This article is licensed under a Creative Commons Attribution 4.0 International License (<https://creativecommons.org/licenses/by/4.0/>), which permits unrestricted use, sharing, adaptation, distribution and reproduction in any medium or format, for any purpose, even commercially, as long as you give appropriate credit to the original author(s) and the source, provide a link to the Creative Commons license, and indicate if changes were made.



dendrite formation, thereby bolstering LIB safety. Our findings demonstrate the potential of using active cathode materials as separator coatings to advance LIB technology with high-energy cathodes.

Keywords: Lithium-ion batteries, separator, NCM811 coating, thermal stability, lithium dendrites

INTRODUCTION

Rechargeable batteries with lithium-ion (LIBs) are in high demand for large-scale applications, including portable electronics^[1,2], electric automobiles^[3-5], and energy storage systems (ESSs)^[6-8]. To meet the demand, various cathodes have been explored to increase the energy density of LIBs^[9-12]. However, higher energy density also means more electrochemically active material^[13,14], which can cause safety problems due to unfavorable reactions during charging and discharging cycles^[15,16]. Moreover, high-energy materials can pose a risk to consumers by triggering fires, explosions, and pollution if the batteries are used in abnormal conditions. Therefore, many studies have focused on improving the performance of battery components^[17], especially the separator, which acts as a key factor for battery thermal stability^[18-20], as it separates the anode and the cathode^[21-23]. Currently, most industrial LIBs use polyolefin separators, such as polypropylene (PP), polyethylene (PE), and their blends due to their suitable chemical stability, reasonable cost, and acceptable mechanical strength^[24-26]. However, these separators have low porosity, and poor wettability, which limit their electrolyte uptake and ionic conductivity^[27,28]. They also have poor thermal stability and low melting points (around 130-170 °C), which compromise the safety of LIBs^[29-32]. One of the effective solutions to the above problems is to coat polyolefin separators with ceramic particles^[33-37]. Ceramic particles, such as SiO₂^[38,39], TiO₂^[40], and Al₂O₃^[41], are often applied on one or both sides of polyolefin separators to enhance their thermal stability and electrolyte absorption. Additionally, 3D imaging and analysis techniques are also employed to demonstrate how pore size distribution, tortuosity, and phase connectivity influence ion transport and reaction kinetics^[42]. However, these electrochemically inert ceramic layers must be thin enough (< 5 μm, typically 1~2 μm) to avoid increasing the dead weight of batteries^[43], and thus show limited improvement in thermal stability and wettability. Therefore, further improvement of ceramic-coated separators is needed.

In this research, we suggest a novel separator design using Ni-rich LiNi_{0.8}Co_{0.1}Mn_{0.1}O₂ (NCM811) as a coating component on PE/Al₂O₃ separators. NCM811 is a high-energy cathode material that has high capacity and energy density but also poses safety risks due to poor thermal stability during repeated cycling, gas evolution, phase transition, and microcracks^[44]. By using NCM811 as a coating material on PE/Al₂O₃ separators, we aim to improve not only the separator properties but also the electrochemical properties and safety of the NCM811 cathode. The NCM811 coating layer is directly coated on PE/Al₂O₃ separators by a simple casting method. Compared with the inert and thin Al₂O₃ coating, the active NCM811 coating on separators can participate in the electrochemical reactions to contribute capacities, which allow applying thicker ceramic layers (> 10 μm) to more efficiently improve the wettability, thermal stability, ionic diffusion, and Li-ion transfer number of separators.

EXPERIMENTAL AND CALCULATION METHODS

The bare PE separator, the Al₂O₃ inert ceramic coated PE separator, and NCM811 were all purchased from Canrd New Energy Technology Co., Ltd. The PE/Al₂O₃ separator has a model of MC112S1D and shows a structure of polyvinylidene fluoride (PVDF)/PE/Al₂O₃/PVDF with a thickness of 1 + 7 + 2 + 1 μm. The bare PE separator has a model MA-EN-SE-0C011E and a thickness of 12 μm. The NCM811 material was milled by a planetary ball mill for 225 min to reduce the particle size [Supplementary Figure 1A]. The NCM811 coated slurry was prepared using PVDF, NCM811, and Ketjen black (KB) dispersed in N-methyl

pyrrolidone (NMP). The weight ratios of NCM811, KB, and PVDF were 90:3:7. The coating slurry was stirred uniformly and coated on a 10 μm thick PE/ Al_2O_3 separator [Supplementary Figure 1B]. The separator was dried in a vacuum oven at 80 $^\circ\text{C}$ for one day. The total thicknesses of NCM-unmilled and NCM-crushed coated separators were about 32 and 28 μm , respectively.

The surface morphologies of the separators were examined by scanning electronic microscopy (SEM). The mechanical strength of the separators was assessed using a mechanical testing system. The separator's thermal stability was evaluated via an infrared thermal imager (FLIR, model A655sc). The thermal shrinkage was determined by measuring the separator's areas before and after heating for 30 min at various temperatures. The electrolyte uptake was determined by measuring the separator's weights before and after being immersed in the electrolyte for 30 min. The separator's wettability was measured by a surface contact angle test. The ionic conductivities at various temperatures were measured by AC impedance spectroscopy.

The electrochemical performance of the NCM811 cathode with different separators was evaluated by assembling coin-type half-cells (CR2032) in an argon-filled glove box. The positive electrode was prepared by mixing NCM811, PVDF, and KB with a weight ratio of 85:10:5. The negative electrode was a lithium metal foil. The electrolyte was 1.0 M LiPF_6 in ethylene carbonate (EC) and ethyl methyl carbonate (EMC) with a weight ratio of 3:7. The cells were cycled between 2.4 and 4.8 V at various current rates using a battery tester (LAND CT2001A). The total active material in both cathode and separator active coatings is included for calculating mass specific capacity. The electrochemical impedance spectroscopy (EIS) measurements were performed on a CHI660E electrochemical workstation in the frequency range from 100 kHz to 10 mHz with an amplitude of 5 mV. The lithium-ion transference number (t_{L^+}) was calculated through the EIS impedance before and after a direct-current (DC) polarization using the electrochemical workstation (DH7001B, DongHua Analytical). The t_{L^+} was calculated at room temperature using:

$$t_{L^+} = \frac{I_s(\Delta V - R_0 I_0)}{I_0(\Delta V - R_s I_s)} \quad (1)$$

where ΔV represents the applied DC polarization voltage (0.01 V) in the chronoamperometric step, and I_0 and I_s denote the initial and steady-state currents, respectively. The initial and steady-state interfacial resistances are denoted by R_0 and R_s , respectively.

The interaction between separator layers was studied by determining the atomic configurations and adsorption energies of PE with Al_2O_3 and NCM811 using density functional theory (DFT) calculation implemented by the Dmol3 package within a generalized gradient approximation (GGA) of the Perdew-Burke-Ernzerhof (PBE) functional. The Double Numeric with polarization (DNP) basis sets with effective core potential were employed for self-consistent field (SCF) calculations with 1×10^{-6} eV/atom SCF tolerance, 1000 Max. SCF cycles, and Gamma K-point was used for molecule and surface model optimization. Butane molecule was used to represent the fragment of the PE polymer chain. $\text{Al}_2\text{O}_3(001)$ surface and NCM(100) were created and optimized before absorption calculation. A small Al_2O_3 cluster was used to calculate the interaction between NCM(100) surface and Al_2O_3 .

RESULTS AND DISCUSSION

As illustrated in Figure 1, the performances of the bare PE separator, Al_2O_3 inert ceramic coated PE separator, and NCM811 active material coated PE/ Al_2O_3 separators are compared under a high-temperature environment. At higher temperatures, as shown in Figure 1A, PE shrinks and melts, causing short circuits

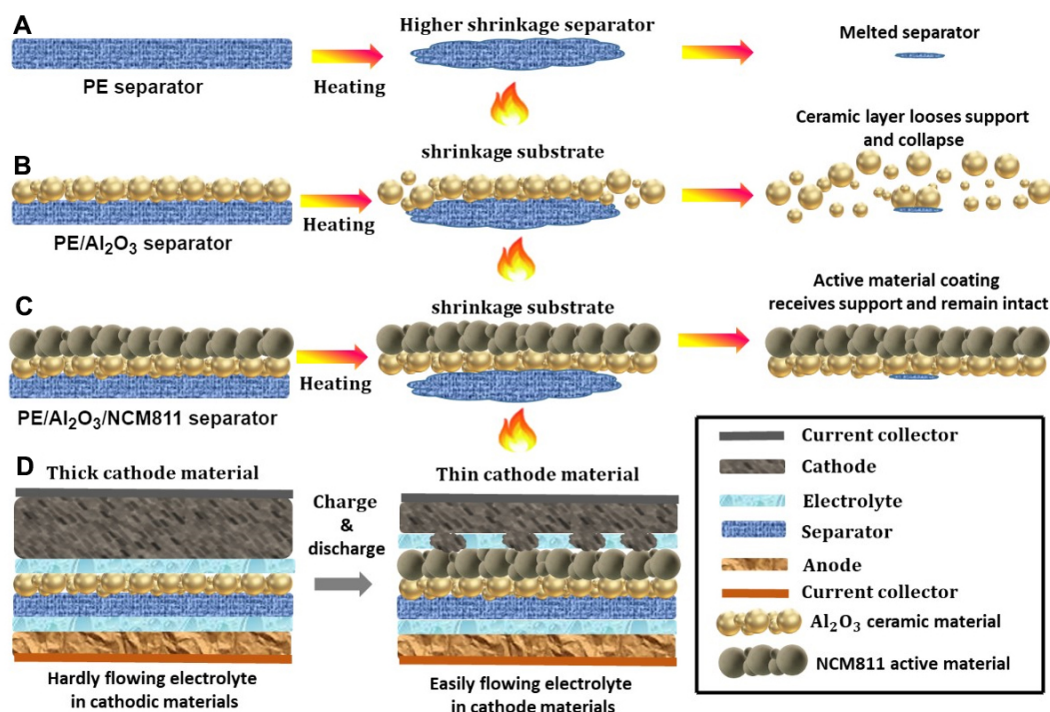


Figure 1. Schematic illustrating diagram of the failure mechanism of high-temperature stability of (A) polyolefin-based separator, (B) inert ceramic-coated separator, (C) active material-coated separator. (D) Schematic illustrating capacity increase by using active material coated separator instead of using a thick cathode.

of cells with pure PE separators. Thin Al₂O₃ ceramic particles in PE/Al₂O₃ separators [Figure 1B] lost their support and collapse. However, the active material particles remain intact and supported by the Al₂O₃ ceramic layer. The active material coating not only has excellent thermal resistance, but also creates a current path and electrochemical reaction due to the physical contact with the cathode, providing additional capacity [Figure 1D].

Supplementary Figure 1 illustrates the ball milling process of NCM811 and the preparation process of NCM811 coated separators. Supplementary Figure 2 shows that the NCM-unmilled powders had a larger average particle size of 5.21 μm with some aggregates of smaller particles. The average particle dimension was reduced from 5.21 μm to 2.64 μm after ball milling. Figure 2 exhibits the SEM images of the surfaces and cross-sections of different separators. The SEM image of the bare PE separator in Figure 2A shows uniform submicron pores. A uniform structured layer was formed when Al₂O₃ was coated on a bare PE separator surface regardless of its shape [Figure 2B]. Similarly, the crushed NCM particles were well distributed when they were coated on a PE/Al₂O₃ composite separator, as shown in Figure 2C. However, the unmilled NCM particles had some small aggregates due to their large size, which might hinder their uniform distribution in the coating layer [Figure 2D]. The energy dispersive X-Ray spectroscopy (EDX) mapping in Supplementary Figure 3 confirms the presence and uniform distribution of NCM811 coating on the PE/Al₂O₃ separator. The cross-sectional image in Figure 2E demonstrates that the bare PE separator had a thickness of 12 μm. The smooth cross-section layer of a PE/Al₂O₃ separator in Figure 2F demonstrates that the Al₂O₃ ceramic material coating layer adhered to the surface of the pure PE separator and the Al₂O₃ layer had a thickness of about 3 μm thick on one side. The coating layers of crushed and unmilled NCM particles in Figure 2G and H were attached securely to the PE/Al₂O₃ ceramic-coated separator and had a thickness of about 18 μm on one side.

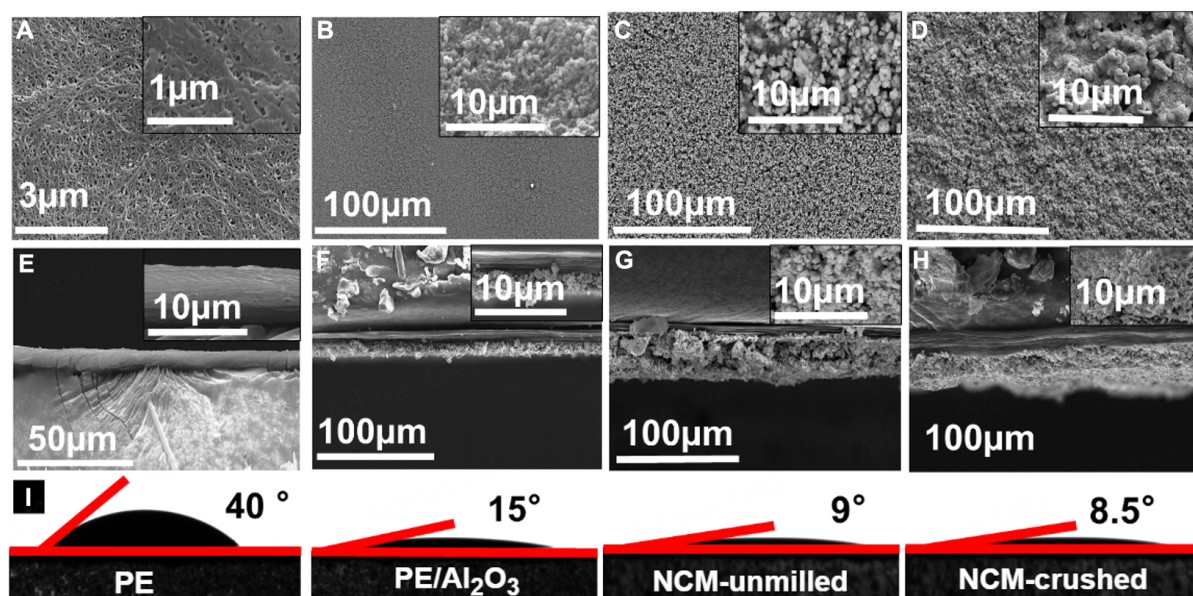


Figure 2. SEM images surface of (A) bare PE, (B) PE/Al₂O₃, (C) NCM-crushed coated, and (D) NCM-unmilled coated separators. Cross-sectional SEM image of (E) bare PE separator, (F) PE/Al₂O₃ separator, (G) NCM-crushed coated separator, and (H) NCM-unmilled separator. (I) Contact angle pictures of different separators.

The separator's wettability was evaluated by measuring the contact angle with the electrolyte and the electrolyte uptake. Figure 2I shows that the Al₂O₃-coated separator was more hydrophilic than the bare PE separator, as its contact angle reduced from 40° to 15° due to the presence of Al₂O₃ ceramic particles on its surface. The NCM-coated separator was even more hydrophilic, with a contact angle of 8.5°, because of the NCM powder's affinity for polar solvents. The electrolyte uptake in Supplementary Table 1 also confirmed this trend. The bare PE separators had low electrolyte uptake because of their hydrophobic nature. While the Al₂O₃-coated separators exhibited higher electrolyte uptake, the NCM coating can further increase electrolyte uptake because of their hydrophilic nature and compatibility with the electrolyte solution. Figure 3A shows the ionic conductivities of bare PE, Al₂O₃-coated PE, and NCM-coated PE/Al₂O₃ separators increased with temperature from 30 to 80 °C. The NCM-coated separator had the highest ionic conductivity at all temperatures. Indicating that Li⁺ ions could move more easily between the electrodes through the electrolyte. Supplementary Table 1 shows the ionic conductivity of several separators at 30 °C. NCM-coated separators had an ionic conductivity of 0.85 mS cm⁻¹, much higher than the 0.49 mS cm⁻¹ of the pure PE separator and the 0.54 mS cm⁻¹ of the Al₂O₃-coated separator. The reason for the enhanced ionic conductivity was the increased electrolyte absorption and wettability of the NCM-coated separator.

The mechanical properties of a separator are important for its industrial applications. Figure 3B compares the mechanical properties of separators. NCM-crushed coated separators had a larger tensile strength of 160.3 MPa than the PE/Al₂O₃ separator (158.5 MPa), as shown in Supplementary Table 1. The NCM-unmilled coated separator had a lower tensile strength and puncture resistance, but a higher elongation, due to the unevenness of the NCM-unmilled particles. Figure 3C and Table 1 show that the NCM-crushed coated separator had a slightly greater puncture property of 4.6 N than the Al₂O₃-coated separator (4.4 N). The thermal stability of separators was evaluated by measuring their shrinkage after being heated for half an hour, as shown in Figure 3D. The pure PE separator had a high thermal shrinkage ratio of 60% at 160 °C, due to its low melting point and isotropic structure. The Al₂O₃-coated PE separator had a lower thermal shrinkage ratio of 26.3% at the same temperature. The NCM-unmilled coated and NCM-crushed coated

Table 1. Summary of cell performance with different separators

Separators	PE	PE/Al ₂ O ₃	NCM-unmilled	NCM-crushed
NCM mass loading on cathode (mg/cm ²)	7.87	7.86	7.93	7.88
NCM mass loading on separator (mg/cm ²)	0	0	2.79	2.77
Discharge capacity (mAh/g)	0.5 C	166.5	178	216.3
	1 C	102.4	134.8	152.8
	2 C	64.5	109.7	120.7
	4 C	24.6	69.2	82.6

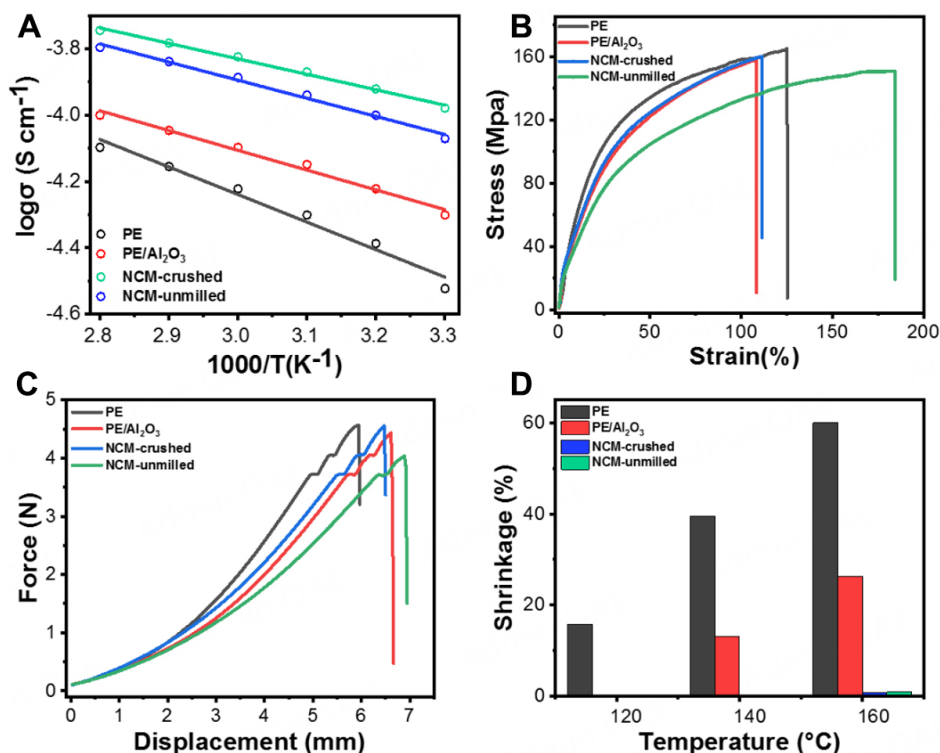


Figure 3. (A) The ionic conductivities of pure PE, PE/Al₂O₃, NCM-crushed and NCM-unmilled separators at different temperatures. (B) Stress-strain profiles of different separators. (C) Force-displacement profiles for punch strength of various separators. (D) Heat shrinkage for different separators under different temperatures.

separators had even lower thermal shrinkage ratios of 1% and 0.8%, respectively, because of the improved thermal stability of the NCM particles.

Figure 4A shows optical images of different separators before and after heating them at 160 °C for 30 min. The pure PE separator shrank significantly. The NCM-unmilled and crushed coated separators, on the other hand, did not change their shape much, because of the thermal stability of NCM. This layer prevented the polyolefin separator's heat shrinkage effectively. Figure 4B shows the infrared images of different separators. The bare PE separator began to shrink at 80 °C and reached its maximum shrinkage at 140 °C, while Al₂O₃-coated separators were stable at 80 °C but began to shrink at 120 °C. NCM-unmilled and crushed separators, however, remained stable even above the melting point of the bare PE separator. The NCM layer on the separators improved their thermal stability, because of the superior thermal performances of NCM811. The separator's physical properties are important for the safety of LIBs, especially for large-scale applications such as electric vehicles^[45]. A combustion experiment was performed

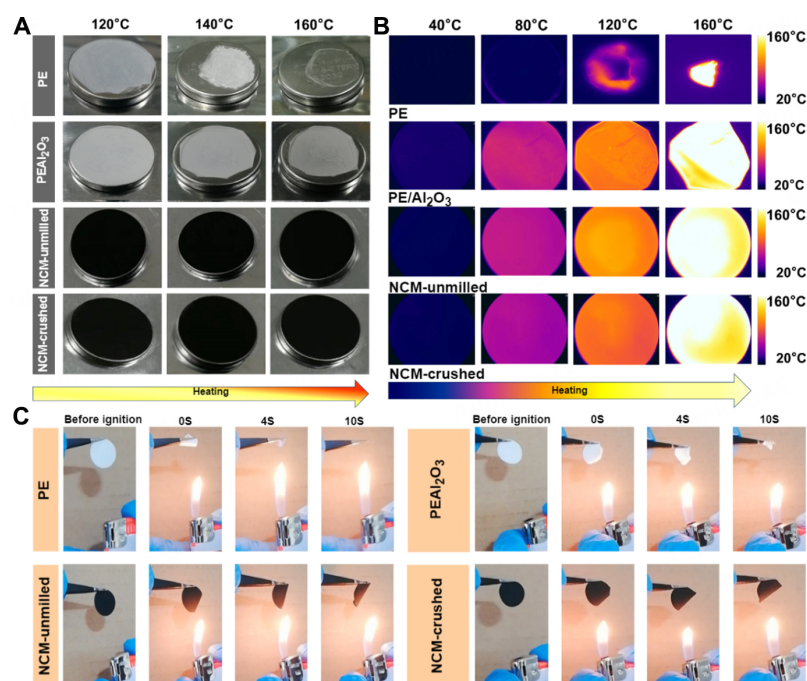


Figure 4. (A) Photographs of bare PE, PE/Al₂O₃, NCM-crushed and NCM-unmilled coated separators after being exposed to the temperature from 120-160 °C for 30 min. (B) FLIR thermal photos of the different separators. (C) Combustion photos of several separators.

to compare the flame retardancy of different separators. Figure 4C shows the images of different separators before, during, and after ignition. The bare PE separator blazed fast and disappeared after ignition. The Al₂O₃-coated separator had better flame retardancy than the PE separator, because of the thermal stability of Al₂O₃ ceramic particles. The NCM-coated separator burned slightly in the flames but did not burn completely, showing its superior flame retardancy and non-flammability. Therefore, the NCM-coated separator enhanced the safety performance of rechargeable batteries by increasing their heat resistance and flame retardancy.

The EIS spectra of the LIB with different separators are shown in Figure 5A. All spectra showed two overlapping semicircles, which represented the resistance of Li⁺ ions through the surface layer on the electrodes and the charge transport resistance at the electrode/electrolyte interface^[46-48]. The cell with the NCM-coated separator had the lowest interface resistances. The cyclic voltammetry (CV) tests were carried out in the voltage range of 2.4-4.7 V at a scan rate of 0.1 mV/ s [Figure 5B]. The CV profiles showed two couple of redox peaks, which corresponded to the redox reaction of Ni²⁺/Ni⁴⁺ in the insertion and extraction of lithium-ions during charge-discharge processes^[49,50]. The potential intervals (ΔE) between the anodic and cathodic peaks reflected the electrochemical process involving electron transfer across the electrodes and lithium-ion diffusion in the electrode/electrolyte interface. The first anodic peak which represented the extraction of lithium-ions and the oxidation of Ni ions and the first cathodic peak which represented the insertion of Li-ions and the reduction of Ni ions of the cell with pure PE separators were at 3.80 and 3.70 V ($\Delta E = 0.10$ V), respectively. The redox peaks of the cell with Al₂O₃-coated separators were at 3.81 and 3.70 V ($\Delta E = 0.11$ V). The redox peaks of the cell with NCM-crushed coated separators were at 3.84 and 3.67 V ($\Delta E = 0.17$ V) while the redox peaks for the cell with NCM-unmilled-coated separators were at 3.88 and 3.69 V ($\Delta E = 0.19$ V). The ΔE values of Li-ion half-cells with pure PE separators were smaller than those of Al₂O₃-coated and NCM-coated separators, suggesting that the coating layers did not affect the

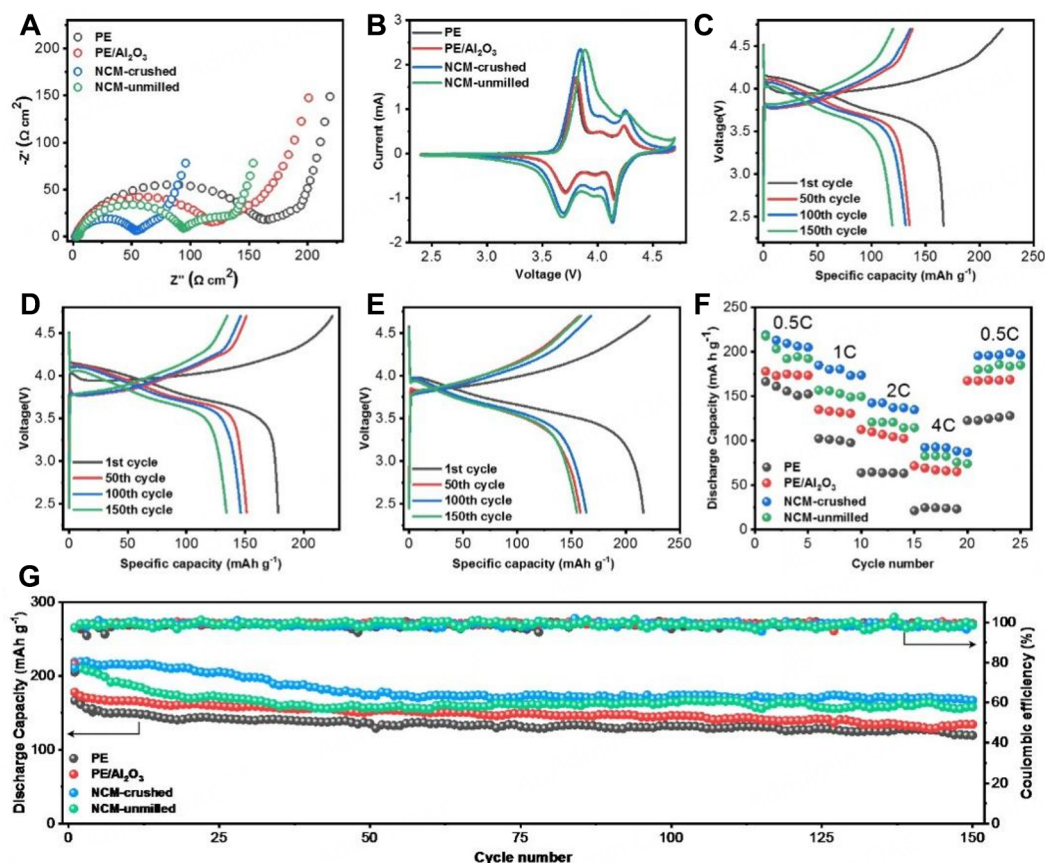


Figure 5. (A) Nyquist plot of NCM811/Li cells with the pure PE separator, Al₂O₃-coated separator, NCM-crushed coated separator, and NCM-unmilled coated separator. (B) Cyclic voltammetry (CV) profiles of NCM811/Li half-cells with various separators. (C-E) Charge/discharge curves of cells between the 1st and 150th cycles at 0.5 C with (C) pure PE separator, (D) PE/Al₂O₃ separator, and (E) NCM-crushed coated separator, respectively. (F) The rate capability of NCM811/Li cells with various separators. (G) Cycling performances of NCM811/Li cells with several separators in the voltage of 2.4–4.7 V at 0.5 C.

electrochemical polarization process of cathode materials. However, the strong cathodic/anodic peaks in the cell with Al₂O₃- and NCM-coated separators suggest that the Li-ion and electron diffusion was faster. The normalized CV curves are shown in [Supplementary Figure 4](#). The NCM-coated separators show higher specific peak currents than the uncoated separators, indicating improved utilization of the active material; the integrated area of the CV curves, which correlates to capacity, is larger for the NCM-coated separators on a per-gram basis.

The charge and discharge curves of cells with different separators after the 1st and 150th cycles at 0.5 C are displayed in [Figure 5C-E](#). The voltage hysteresis increased during the charge and discharge process as the cycling increased for all cells. However, the cells with bare PE separators and PE/Al₂O₃ separators exhibited low discharge capacities compared to the cells with NCM-coated separators. The initial discharge capacities at 0.5 C within 2.4–4.7 V were 166.5, 178, 219.03 and 216.32 mAh g^{-1} for the bare PE separator, PE/Al₂O₃ separator, NCM-crushed coated separator, and NCM-unmilled coated separator, respectively. After 150 cycles, the cell discharge capacities were 119.3, 134, 166.7 and 157.56 mAh g^{-1} for the same separators, respectively. The cell with the NCM-crushed coated separator showed the largest discharge capacity even after 150 cycles compared to cells with the other separators. [Figure 5F](#) shows the discharge capacities at different C rates from 0.5 to 4.0 C, changing every five cycles. The relative capacity in this figure is calculated as the difference between the starting discharge capacity at 0.5 C and the discharge capacity at a

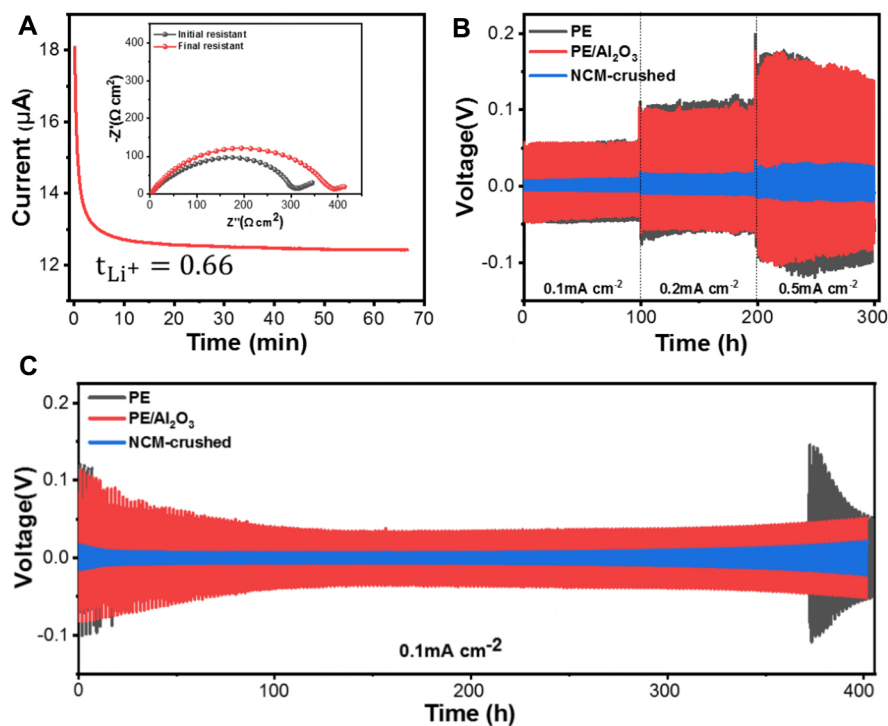


Figure 6. (A) Chronoamperometric of the Li||NCM-crushed||Li cell with a potential step of 0.01 V. (B) rate performances at 0.1, 0.2 and 0.5 mA cm^{-2} . (C) cycle stability Li plating/stripping property with different separators at 0.5 mA cm^{-2} .

given C-rate. The cell using the NCM-coated separator exhibited the highest discharge capacities for all the C-rates compared to the cells using bare PE or PE/ Al_2O_3 separators, which agreed with the highest ionic conductivity of the NCM-coated separator. Figure 5G shows the cycling capabilities of the cells with various separators at 0.5 C. The capacity retentions of the cell with the bare PE separator, the Al_2O_3 -coated separator, the NCM-crushed coated separator, and the NCM-unmilled coated separator are 71.6%, 75.3%, 76.1%, and 72.8%, respectively. The cell with an NCM-crushed coated separator exhibits the highest capacity retention compared with the cells with other separators. This was due to the strong interaction between the NCM-crushed layer and the ceramic Al_2O_3 particle layer. The performances of the cells with various separators are summarized in Table 1. The calculation of cell capacity has included the total mass of active material from both the cathode and the active coating on a separator. The mass loading of NCM on the cathode ranges from 7.87 to 7.93 mg cm^{-2} , while on the separator, it ranges from 2.77 to 2.79 mg cm^{-2} . This indicates that the NCM coating on the separator adds approximately 35% more active material compared to the cathode alone. Supplementary Figure 5 provides charge/discharge profiles of three cells with different configurations and illustrates that NCM811 coating on the separator participates in the electrochemical reaction and contributes additional cell capacity. A comparative analysis of the estimated cost of the various separators is presented in Supplementary Table 1.

The Li-ion transference, which indicates the electrolyte's ability to Li-ion transport, was analyzed. A higher Li-ion transference can prevent the lithium dendrite growth and increase the battery capacity and cycle life^[51,52]. As shown in Figure 6A, the cell using NCM-coated separators showed a larger t_{Li^+} of 0.66 compared to those using the bare PE and PE/ Al_2O_3 separators, which had t_{Li^+} of 0.31 and 0.43, respectively. Figure 6B shows the overpotential of the Li/Li cells with various separators at different current densities of 0.1, 0.2, and 0.5 mA/cm^2 . The overpotential increased with the current density for all cells. The Li/Li cells with bare PE

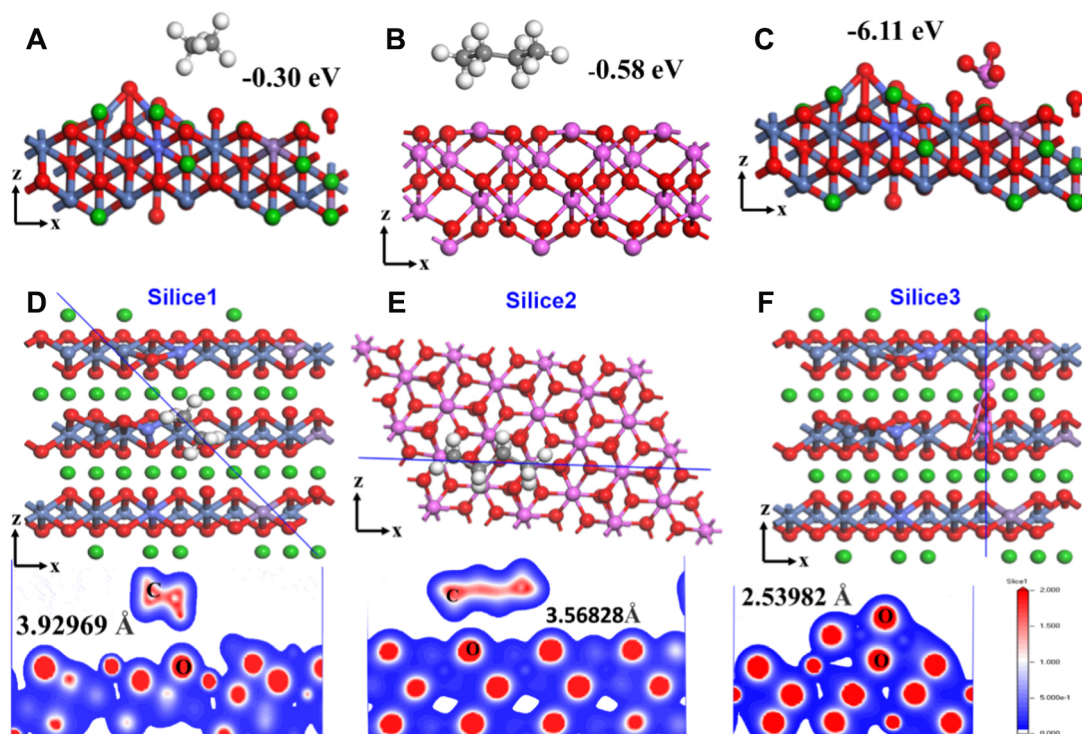


Figure 7. Absorption energy calculation of the PE, Al_2O_3 and NCM811 in the separator: (A) PE and NCM(100). (B) PE and Al_2O_3 (001). (C) Al_2O_3 and NCM(100). Slices of the electron density distribution: (D) PE and NCM(100). (E) PE and Al_2O_3 (001). (F) Al_2O_3 and NCM(100). In the Figure, the gray, white, green, red, steel blue, slate blue, medium purple and pink balls represent C, H, Li, O, Ni, Co, Mn and Al, respectively.

and PE/ Al_2O_3 separators had similar overpotential under 300 hours at distinct current densities, while the cells with NCM-crushed separators displayed lower overpotential at the same current densities. The cycling performance of Li/Li symmetric cells with different separators was evaluated to assess their ability to suppress the Li dendrite growth [Figure 6C]. The Li/Li cells with the bare PE and PE/ Al_2O_3 separators at 0.1 mA cm^{-2} showed more fluctuations in voltages than the Li/Li cells using NCM-crushed coated separators, indicating the Li dendrite growth during cycling. However, the cell with the NCM-crushed coated separator had a stable and a small overpotential during the cycling under 400 h and also shows cycling uniformity from 0 to 400 h than the other cells. This was because of the high ionic conductivity, good interfacial adhesion with the anode, strong mechanical strength, and unified Li^+ flux by NCM-crushed coating. These findings agree with previous research by Yang *et al.*^[52]. When using Li/Li cells to test the dendrite performance, direct contact between the NCM811 coating on the separator contact Li metal can induce phase change or reactions. However, the results still show that NCM811 layers effectively suppress Li dendrite growth. In actual Li/NCM half-cell or graphite/NCM full-cell configurations, the NCM coating on the separator will face the cathode side. The Al_2O_3 layer and the PE base separator will separate the NCM811 coating from the anode, avoiding any side reactions or phase changes between NCM811 and Li.

DFT computations were used to study the interface interaction of the PE/ Al_2O_3 /NCM811-coated separator and the impact of the Al_2O_3 and NCM811 layers. Figure 7A-C displays the calculated adsorption energies of PE-NCM811(100) surface, PE- Al_2O_3 (100) surface, and Al_2O_3 -NCM811(100) surface, respectively. The results show that PE- Al_2O_3 has a higher adsorption energy of -0.58 eV than PE-NCM811(-0.30 eV). However, the adsorption energy increases significantly to -6.11 eV between NCM811 and Al_2O_3 , indicating a strong interfacial interaction between them. Therefore, the strong interfacial interactions of PE- Al_2O_3 and

Al₂O₃-NCM811 confirm the high mechanical proprieties and thermal stability of the PE/Al₂O₃/NCM811 separator, which ensures the electrochemical proprieties of NCM811/Li cells. Figure 7D-F also shows the strong interfacial contacts of the layers by the bonding electron cloud between atoms for each layer such as PE-NCM811 (C-O, 3.93 Å), PE- Al₂O₃ (C-O, 3.57 Å), and Al₂O₃-NCM811 (O-O, 2.54 Å). The stronger the binding between the atoms of Al₂O₃ and NCM811, the more stable their layers become, enhancing the interfacial interactions between layers and the integrity of the pore framework of the PE/Al₂O₃/NCM811 separator. The DFT results were consistent with our experimental measurements.

CONCLUSIONS

In this work, we have developed a novel separator design using NCM811 as a coating material on PE/Al₂O₃ separators for improving the performance and safety of LIBs with high-energy cathodes. The NCM811 coating layer was directly cast on PE/Al₂O₃ separators. This layer enhances wettability, thermal stability, ionic conductivity, and Li-ion transfer number of the PE/Al₂O₃ separator. The NCM811|Li half-cell with NCM811-coated separators showed higher capacity retention and better rate performance than those with PE or PE/Al₂O₃ separators. The NCM811 coating layer also prevented the growth of lithium dendrites on the anode surface during cycling, which enhanced the safety of LIBs. This work demonstrated that using active cathode material as a coating layer on a separator was an effective strategy to improve the performance and safety of LIBs with high-energy cathodes. This work also provided a new perspective for designing separators with active materials for various battery systems.

DECLARATIONS

Authors' contributions

Investigation, data curation, formal analysis, writing - original draft: Nitou, M. V. M.

Investigation, data curation, writing - review & editing: Fang, X.; Liu, R.; Pang, Y.

Software, simulation, data curation, writing - review & editing: Wang, J.; Qin, W.

Formal analysis, writing - review & editing: Zhang, Z.

Supervision, administration, funding, validation, writing - review & editing: Niu, Y.; Zhao, C.; Chen, Y.; Lv, W.

Availability of data and materials

The raw/processed data required to reproduce these findings cannot be shared at this time due to technical or time limitations.

Financial support and sponsorship

This work was supported by the Natural Science Foundation of China (Grant Nos. 51972043 and 52102212), the fellowship of China Postdoctoral Science Foundation (No. 2022M720653), the Sichuan-Hong Kong Collaborative Research Fund (No. 2021YFH0184) and the Natural Science Foundation of Sichuan Province (Nos. 2023NSFSC0417 and 2023NSFSC0974).

Conflict of interest

All authors declared that there are no conflicts of interest.

Ethical approval and consent to participate

Not applicable.

Consent for publication

Not applicable.

Copyright

© The Author(s) 2025.

REFERENCES

1. Rajaeifar, M. A.; Ghadimi, P.; Raugei, M.; Wu, Y.; Heidrich, O. Challenges and recent developments in supply and value chains of electric vehicle batteries: a sustainability perspective. *Resour. Conserv. Recy.* **2022**, *180*, 106144. DOI
2. Zuo, W.; Innocenti, A.; Zarrabeitia, M.; Bresser, D.; Yang, Y.; Passerini, S. Layered oxide cathodes for sodium-ion batteries: storage mechanism, electrochemistry, and techno-economics. *ACC. Chem. Res.* **2023**, *56*, 284-96. DOI PubMed PMC
3. Murugan, M.; Saravanan, A.; Elumalai, P. V.; et al. Thermal management system of lithium-ion battery packs for electric vehicles: an insight based on bibliometric study. *J. Energy. Storage.* **2022**, *52*, 104723. DOI
4. Khan, F. M. N. U.; Rasul, M. G.; Sayem, A. S. M.; Mandal, N. K. Design and optimization of lithium-ion battery as an efficient energy storage device for electric vehicles: a comprehensive review. *J. Energy. Storage.* **2023**, *71*, 108033. DOI
5. Chen, S.; Xiong, J.; Qiu, Y.; Zhao, Y.; Chen, S. A bibliometric analysis of lithium-ion batteries in electric vehicles. *J. Energy. Storage.* **2023**, *63*, 107109. DOI
6. Qiu, Y.; Dong, T.; Lin, D.; Zhao, B.; Cao, W.; Jiang, F. Fault diagnosis for lithium-ion battery energy storage systems based on local outlier factor. *J. Energy. Storage.* **2022**, *55*, 105470. DOI
7. Liu, W.; Cao, J.; Song, F.; et al. A double transition metal $Ti_2NbC_2T_x$ MXene for enhanced lithium-ion storage. *Rare. Met.* **2023**, *42*, 100-10. DOI
8. Nian, Q.; Sun, T.; Liu, S.; Du, H.; Ren, X.; Tao, Z. Issues and opportunities on low-temperature aqueous batteries. *Chem. Eng. J.* **2021**, *423*, 130253. DOI
9. Jyoti, J.; Singh, B. P.; Tripathi, S. K. Recent advancements in development of different cathode materials for rechargeable lithium ion batteries. *J. Energy. Storage.* **2021**, *43*, 103112. DOI
10. Zhao, S.; Guo, Z.; Yan, K.; et al. Towards high-energy-density lithium-ion batteries: strategies for developing high-capacity lithium-rich cathode materials. *Energy. Storage. Mater.* **2021**, *34*, 716-34. DOI
11. Chu, B.; Guo, Y. J.; Shi, J. L.; et al. Cobalt in high-energy-density layered cathode materials for lithium ion batteries. *J. Power. Sources.* **2022**, *544*, 231873. DOI
12. Teng, J.; Tang, X.; Li, H.; Wu, Q.; Zhao, D.; Li, J. Al-Li alloys as bifunctional sacrificial lithium sources for prelithiation of high-energy-density Li-ion batteries. *J. Power. Sources.* **2022**, *540*, 231642. DOI
13. Zhang, X.; Hui, Z.; King, S.; et al. Tunable porous electrode architectures for enhanced Li-ion storage kinetics in thick electrodes. *Nano. Lett.* **2021**, *21*, 5896-904. DOI
14. Chang, J. H.; Pin, M. W.; Kim, I.; et al. Binder migration: frequently observed yet overlooked phenomena in electrode processing for lithium-ion batteries. *J. Energy. Storage.* **2024**, *83*, 110729. DOI
15. Ogihara, N.; Itou, Y.; Sasaki, T.; Takeuchi, Y. Impedance spectroscopy characterization of porous electrodes under different electrode thickness using a symmetric cell for high-performance lithium-ion batteries. *J. Phys. Chem. C.* **2015**, *119*, 4612-9. DOI
16. Wang, J.; Sun, Q.; Gao, X.; et al. Toward high areal energy and power density electrode for Li-ion batteries via optimized 3D printing approach. *ACS. Appl. Mater. Interfaces.* **2018**, *10*, 39794-801. DOI
17. Liu, Z.; Jiang, Y.; Hu, Q.; et al. Safer lithium-ion batteries from the separator aspect: development and future perspectives. *Energy. Environ. Mater.* **2021**, *4*, 336-62. DOI
18. Huang, Z.; Chen, Y.; Han, Q.; et al. Vapor-induced phase inversion of poly (m-phenylene isophthalamide) modified polyethylene separator for high-performance lithium-ion batteries. *Chem. Eng. J.* **2022**, *429*, 132429. DOI
19. Yu, B.; Chen, X.; Jin, X.; Zhang, X.; Chen, L. Heat-resistant lithium-ion-battery separator using synchronous thermal stabilization/imidization. *ACS. Appl. Polym. Mater.* **2024**, *6*, 2464-73. DOI
20. Lagadec, M. F.; Zahn, R.; Wood, V. Characterization and performance evaluation of lithium-ion battery separators. *Nat. Energy.* **2019**, *4*, 16-25. DOI
21. Deng, J.; Cao, D.; Yang, X.; Zhang, G. Cross-linked cellulose/carboxylated polyimide nanofiber separator for lithium-ion battery application. *Chem. Eng. J.* **2022**, *433*, 133934. DOI
22. Min, Y.; Guo, L.; Wei, G.; Xian, D.; Zhang, B.; Wang, L. Enhancing the safety and cyclic performance of lithium-ion batteries using heat resistant and wettable separator based on covalent organic framework and polybenzimidazole. *Chem. Eng. J.* **2022**, *443*, 136480. DOI
23. Zhong, S.; Yuan, B.; Guang, Z.; et al. Recent progress in thin separators for upgraded lithium ion batteries. *Energy. Storage. Mater.* **2021**, *41*, 805-41. DOI
24. Long, M. C.; Duan, P. H.; Gao, Y.; Wang, X. L.; Wu, G.; Wang, Y. Z. Boosting safety and performance of lithium-ion battery enabled by cooperation of thermotolerant fire-retardant composite membrane and nonflammable electrolyte. *Chem. Eng. J.* **2022**, *432*, 134394. DOI
25. Yu, Y.; Jia, G.; Zhao, L.; et al. Flexible and heat-resistant polyphenylene sulfide ultrafine fiber hybrid separators for high-safety lithium-ion batteries. *Chem. Eng. J.* **2023**, *452*, 139112. DOI
26. Babiker, D. M. D.; Usha, Z. R.; Wan, C.; Hassaan, M. M. E.; Chen, X.; Li, L. Recent progress of composite polyethylene separators for lithium/sodium batteries. *J. Power. Sources.* **2023**, *564*, 232853. DOI

27. Han, C.; Cao, Y.; Zhang, S.; et al. Separator with nitrogen-phosphorus flame-retardant for $\text{LiNi}_x\text{Co}_y\text{Mn}_{1-x-y}\text{O}_2$ cathode-based lithium-ion batteries. *Small* **2023**, *19*, e2207453. DOI
28. Nitou, M. V. M.; Tang, M.; Niu, Y.; et al. Separator with active coating for fast and stable Li-ion batteries. *J. Power. Sources.* **2024**, *602*, 234406. DOI
29. Dong, G.; Liu, B.; Kong, L.; et al. Neoteric polyimide nanofiber encapsulated by the TiO_2 armor as the tough, highly wettable, and flame-retardant separator for advanced lithium-ion batteries. *ACS. Sustain. Chem. Eng.* **2019**, *7*, 17643-52. DOI
30. Ding, L.; Zhang, C.; Wu, T.; et al. Effect of temperature on compression behavior of polypropylene separator used for Lithium-ion battery. *J. Power. Sources.* **2020**, *466*, 228300. DOI
31. Lu, Z.; Sui, F.; Miao, Y. E.; et al. Polyimide separators for rechargeable batteries. *J. Energy. Chem.* **2021**, *58*, 170-97. DOI
32. Lingappan, N.; Lee, W.; Passerini, S.; Pecht, M. A comprehensive review of separator membranes in lithium-ion batteries. *Renew. Sustain. Energy. Rev.* **2023**, *187*, 113726. DOI
33. Parikh, D.; Jafra, C. J.; Thapaliya, B. P.; et al. $\text{Al}_2\text{O}_3/\text{TiO}_2$ coated separators: roll-to-roll processing and implications for improved battery safety and performance. *J. Power. Sources.* **2021**, *507*, 230259. DOI
34. Wu, S.; Ning, J.; Jiang, F.; Shi, J.; Huang, F. Ceramic nanoparticle-decorated melt-electrospun PVDF nanofiber membrane with enhanced performance as a lithium-ion battery separator. *ACS. Omega.* **2019**, *4*, 16309-17. DOI PubMed PMC
35. Wang, W.; Yuan, Y.; Wang, J.; et al. Enhanced electrochemical and safety performance of lithium metal batteries enabled by the atom layer deposition on PVDF-HFP separator. *ACS. Appl. Energy. Mater.* **2019**, *2*, 4167-74. DOI
36. Valverde, A.; Gonçalves, R.; Silva, M. M.; et al. Metal-organic framework based PVDF separators for high rate cycling lithium-ion batteries. *ACS. Appl. Energy. Mater.* **2020**, *3*, 11907-19. DOI
37. Babiker, D. M. D.; Wan, C.; Mansoor, B.; et al. Superior lithium battery separator with extraordinary electrochemical performance and thermal stability based on hybrid UHMWPE/ SiO_2 nanocomposites via the scalable biaxial stretching process. *Compos. Part. B. Eng.* **2021**, *211*, 108658. DOI
38. Park, J.; Kwon, Y. J.; Yun, J.; et al. Ultra-thin SiO_2 nanoparticle layered separators by a surface multi-functionalization strategy for Li-metal batteries: highly enhanced Li-dendrite resistance and thermal properties. *Energy. Storage. Mater.* **2024**, *65*, 103135. DOI
39. Feng, G.; Li, Z.; Mi, L.; Zheng, J.; Feng, X.; Chen, W. Polypropylene/hydrophobic-silica-aerogel-composite separator induced enhanced safety and low polarization for lithium-ion batteries. *J. Power. Sources.* **2018**, *376*, 177-83. DOI
40. Zhang, S. S.; Fan, X.; Wang, C. Preventing lithium dendrite-related electrical shorting in rechargeable batteries by coating separator with a Li-killing additive. *J. Mater. Chem. A.* **2018**, *6*, 10755-60. DOI
41. Hyun, D. E.; Jung, Y. J.; Kim, T. W.; et al. Multi-functional Al_2O_3 -coated separators for high-performance lithium-ion batteries: critical effects of particle shape. *Ceram. Int.* **2023**, *49*, 30147-55. DOI
42. Khan, Z. A.; Salaberri, P. A. G.; Heenan, T. M. M.; et al. Probing the structure-performance relationship of lithium-ion battery cathodes using pore-networks extracted from three-phase tomograms. *J. Electrochem. Soc.* **2020**, *167*, 040528. DOI
43. Roh, Y.; Jin, D.; Kim, E.; et al. Highly improved thermal stability of the ceramic coating layer on the polyethylene separator via chemical crosslinking between ceramic particles and polymeric binders. *Chem. Eng. J.* **2022**, *433*, 134501. DOI
44. Feng, Z.; Rajagopalan, R.; Sun, D.; Tang, Y.; Wang, H. In-situ formation of hybrid Li_3PO_4 - AlPO_4 - $\text{Al}(\text{PO}_3)_3$ coating layer on $\text{LiNi}_{0.8}\text{Co}_{0.1}\text{Mn}_{0.1}\text{O}_2$ cathode with enhanced electrochemical properties for lithium-ion battery. *Chem. Eng. J.* **2020**, *382*, 122959. DOI
45. Kim, M.; Park, J. H. Inorganic thin layer coated porous separator with high thermal stability for safety reinforced Li-ion battery. *J. Power. Sources.* **2012**, *212*, 22-7. DOI
46. Liu, T.; Garsuch, A.; Chesneau, F.; Lucht, B. L. Surface phenomena of high energy $\text{Li}(\text{Ni}_{1/3}\text{Co}_{1/3}\text{Mn}_{1/3})\text{O}_2$ /graphite cells at high temperature and high cutoff voltages. *J. Power. Sources.* **2014**, *269*, 920-6. DOI
47. Jin, X.; Cai, Z.; Zhang, X.; et al. Transferring liquid metal to form a hybrid solid electrolyte via a wettability-tuning technology for lithium-metal anodes. *Adv. Mater.* **2022**, *34*, e2200181. DOI
48. Shin, W. K.; Kannan, A. G.; Kim, D. W. Effective suppression of dendritic lithium growth using an ultrathin coating of nitrogen and sulfur codoped graphene nanosheets on polymer separator for lithium metal batteries. *ACS. Appl. Mater. Interfaces.* **2015**, *7*, 23700-7. DOI PubMed
49. Xiong, C.; Liu, F.; Gao, J.; Jiang, X. One-spot facile synthesis of single-crystal $\text{LiNi}_{0.5}\text{Co}_{0.2}\text{Mn}_{0.3}\text{O}_2$ cathode materials for Li-ion batteries. *ACS. Omega.* **2020**, *5*, 30356-62. DOI PubMed PMC
50. Li, J.; Yao, R.; Cao, C. $\text{LiNi}_{1/3}\text{Co}_{1/3}\text{Mn}_{1/3}\text{O}_2$ nanoplates with {010} active planes exposing prepared in polyol medium as a high-performance cathode for Li-ion battery. *ACS. Appl. Mater. Interfaces.* **2014**, *6*, 5075-82. DOI
51. Kim, D.; Liu, X.; Yu, B.; et al. Amine-functionalized boron nitride nanosheets: a new functional additive for robust, flexible ion gel electrolyte with high lithium-ion transference number. *Adv. Funct. Mater.* **2020**, *30*, 1910813. DOI
52. Yang, L. Y.; Cao, J. H.; Liang, W. H.; Wang, Y. K.; Wu, D. Y. Effects of the separator MOF- Al_2O_3 coating on battery rate performance and solid-electrolyte interphase formation. *ACS. Appl. Mater. Interfaces.* **2022**, *14*, 13722-32. DOI PubMed